RSC Advances

ROYAL SOCIETY OF CHEMISTRY

www.rsc.org/advances

Atomistic level molecular dynamics simulation on the solubilization mechanism of aromatic molecules in anionic micelle

Sourav Mondal [a], Sudipto Ghosh [b], Sirshendu De [a,*]

[a] *Department of Chemical Engineering, Indian Institute of Technology Kharagpur, Kharagpur – 721302, India.*

[b] *Department of Metallurgical and Materials Engineering, Indian Institute of Technology Kharagpur, Kharagpur – 721302, India.*

* Corresponding Author

Tel: + 91 – 3222 – 283926

Fax: +91 – 3222 – 255303

e-mail: sde@che.iitkgp.ernet.in

Abstract

Molecular dynamics simulation of micelle-organic complex reveals interesting insights into solubilization and stability of such systems. Various interpretations based on measurement of size, solubilization isotherm, time resolved fluorescence decay, etc., provide qualitative information about solubilization of organic molecules, mostly benzene and alkanols. The present simulation, based on all-atom CHARMM force-field parameters analyzes the solubilization mechanism. It is observed that solubilization of benzene and toluene occurs in the palisade and inner core of the micelle. Polar aromatics such as pyridine and phenol are solubilized in the micelle-water interface and Stern layer. The hydrophobicity, polarity and size of the aromatic molecule influence solubilization. Thermodynamic free energy and entropy change of the system are responsible for deformation in shape of the micelle and its binding efficiency. The present work helps in selection of surfactant-solute pair and fundamental understanding of the micellar enhanced ultrafiltration process for removal of toxic organic components from water.

Keywords: CHARMM; molecular dynamics; sodium dodecylsulfate; aromatic molecule; solubilization; free energy.

1.0 Introduction

Self assembly is a spontaneously reversible association of small entities, due to the imbalance of the attractive (such as van der Waals force, solvation effects, hydrophobic interactions, bridging effects, etc.) and repulsive forces (electric double layers, hydration effects, steric forces, etc.) at the molecular level. Self assembled processes lead to non-hierarchical structures resulting to micelle formation. Typically, the self assembled aggregates exhibit new functionalities in contrast to their individual monomeric units. The phenomenon of micellization is a thermodynamically driven process having the ability of self

re-organization and formation of a hydrophobic interior core. The head of an ionic micelle is orientated towards water molecule in a micelle. The hydrophobic internal environment solubilizes any non-polar solutes present in the medium.

The study of the shape and structure of various micellar systems in aqueous solution using molecular dynamics simulation has been reported by several researchers in the last couple of years.[1-3] There have been several reports of molecular simulation using sodium dodecylsulfate (SDS) surfactant to investigate the aggregation behavior at solid-liquid,[4] at liquid-liquid and liquid-vapor interfaces,[5] aggregation with carbon nanotubes,[6] self assembly with nanoparticle at liquid-liquid interface,[7] aggregation on graphite[8] and the behavior of water molecules[9] and counterions.[10] The solubilization of oil in surfactant solution has been studied by Karaborni et al., using coarse-grained molecular dynamics solution.[11] They have suggested that transfer of oil molecules from oil phase to micelle is a three step mechanism. These are dissolution of oil in the solvent, exchange of oil molecules from oil droplet to micelle with a collision followed by desorption of surfactants and oils from the oil droplet surface.

Solvation dynamics of coumarin 480 in anionic micelles has been reported by Sarkar et al., based on time dependent stokes shift.[12] Their results reveal that the organic solute resides in the Stern layer of the micelles and the dynamics of the water molecules in the Stern layer is different from the bulk. The solubilization isotherm of benzene and toluene in SDS micelle solution has been reported by Gadelle et al.,[13] using head space gas chromatography. They have concluded that the molecular size and ionic strength of the solution affect the solubilization. Also, the extent of solubilization decreases with solute concentration. Solubilization of aromatic hydrocarbons such as pyrene in different micellar systems has been analyzed by Lianos et al.[14] They have observed weak interaction of organic molecules

with the ionic micelles which is responsible for quick solubilization. The solubilization time is also affected by the size and shape of the micelle. Solubilization of phenolic compounds in cationic micelles has been presented by Kandori et al.[15] They observed that the micelles swell on addition of phenol and it is significantly greater than addition of benzene. Also, there is a distinct demarcation of the solubilization site of benzene and phenol in the micelle.

The relative degree of binding of different counterions to SDS micellar system has been already analyzed using molecular dynamics simulation.[16] The relative priority of the attachment (or stability) of different solutes is quantified based on differential weighting of various thermodynamic parameters of the micelle-counterion system. However, the study of solubilization dynamics of organic solutes in micellar systems has not been explored. In case of micelle-organic system, solubilization site and its implications on the micelle structure play an important role on the degree of binding. In the present study, the solubilization of different aromatic solutes in micellar aggregates is analyzed. The choice of aromatic solutes is based on their level of toxicity in waste water. The information generated from this study would be helpful in understanding the solubilization of organics in micellar enhanced ultrafiltration.[17, 18] The objectives of the present study can, therefore, be listed as:

(1) Precise information about the solubilization site of the organic solutes in the micelle, as the location determines the overall interaction and extent of solubilization.

(2) Interpretation of the size of the micelles due to addition of the organic solutes, as the solubilized polar aromatic molecule tends to distort the self-assembly.

(3) Thermodynamic stability of the organic-surfactant system based on their free energy change, which is responsible for the solubilization and subsequent removal by micellar enhanced ultrafiltration.

(4) The degree of hydration of the organic molecules present in the micellar system.

2.0 Molecular Dynamics Implementation

The surfactant monomer considered is SDS, having a molecular weight of 288.38 g/mol. The transferable intermolecular potential 3-point (TIP3P) model is used to describe the water–water and solute–water interactions.[19] TIP3P uses atom-centered point charges to represent the electrostatic interactions. A water box consisting of 21952 TIP3P water molecules is set up,[20] having a size of 84 x 84 x 84 $\overset{o}{A}^3$. The counterions are added in equimolar proportion with the surfactant concentration, depending on their valence, to maintain electroneutrality of the solution. For the surfactant, the standard all atom lipid residue CHARMM force field is used.[21] For the organic solutes, the CHARMM General Force Field (CGENFF) has been applied.[22, 23] The van der Waals interactions are based on Lennard-Jones (L-J) 6-12 potential:

$$V_{LJ} = 4\varepsilon\left[\left(\frac{\sigma}{r}\right)^{12} - \left(\frac{\sigma}{r}\right)^{6}\right] \quad (1)$$

where, ε is the well depth, σ is the collision diameter and r is the inter-atomic distance. The L-J parameters used in the present simulation for the different counterions are presented in Table 1. Among the four systems (SDS-water-organic), the case where the highest number of water molecules are deleted (due to atomic clashes and overlapping) are selected and an equivalent number of water molecules are deleted from the remaining systems. In this present situation, the SDS-phenol have highest number of atomic clashes with water molecules (13). So, 13 water molecules are removed from all the molecular systems having different organics. Geometric average is taken by combination rules setting L-J interaction parameters between metal and surfactant atoms. The molecular dynamic simulations are performed with

the help of parallel architecture using 32 cores by utilization of the CHARMM v35b6 package.[24]

Table 1: Physical properties of the organic molecules

Molecule	Molecular formulae (weight)	Size $\left(\overset{o}{A}^3\right)$	Log P (octanol-water partition co-efficient)	Solubility in water (g/l)	Relative Polarity (polarity of water- 1)[25]
Benzene	C_6H_6 (78.11)	146 [13]	2.03 [26]	1750	0.111
Toluene	C_7H_8 (92.14)	176 [13]	2.51 [26]	526	0.099
Phenol	C_6H_6O (94.11)	-	1.64 [27]	8280	0.701
Pyridine	C_5H_5N (79.1)	-	0.7 [27]	infinite	0.302

The particle mesh Ewald summation is invoked for calculating the electrostatic interaction with 72 grid points spaced in the unit cell.[28] The kappa value corresponding to the width of the Gaussian distribution central to the Ewald method is set to 0.34. The van der Waals interactions are computed with a band-range cutoff scheme with 8 and 10 A˚ cutoff radii. The minimum distance of closeness between any two atoms is restricted to $1.0\,\overset{o}{A}$. The atom pair list is updated whenever an atom is displaced more than $2\,\overset{o}{A}$ since the last list-update. The van der Waals and electrostatic interactions between two atoms bonded to a common atom (1-2 interaction), 1-3 interaction atoms are excluded from the calculation of energy and forces. A constant dielectric equal to 1.0 is defined over the simulation space. The bond lengths are constrained by the SHAKE algorithm.[29]

The coordinates of the atoms are first minimized by 1000 steps of a steepest descent (SD) energy minimization algorithm[30] followed by 1000 steps of adopted basis Newton Raphson (ABNR) algorithm[31] to resolve any undesirable close contacts between the different components of the system. The system is heated to a temperature of 300 K in 1 ns of 0.001 ps

time step each. The temperature is increased by 2 K, starting from 100 K, after every 10 ps. During the process of heating, the velocities of the molecules are scaled from an initial coordinate set of a uniform Gaussian distribution of the kinetic energy. The rotation of the molecules is stopped after every 10 steps of heating.

Dynamic simulation is performed in a cubic box, with periodic boundary conditions[32] for 5 ns, using the leap-frog verlet algorithm.[33] The time step of simulation is 0.001 ps. During the simulation, the temperature of the system is set to 300 K and pressure to 1 atm.[34] The Berendsen coupling method[35] is used to couple the systems to the heat bath with constant temperature of 300 K. Finally, based on the evolution of the phase space, the potential energy of the system, profile of inter atomic distance, free energy change, hydration number, solvent accessible surface area and radial distribution functions are computed.

The final configuration of the equilibrated structure is independent on the initial configuration. Only the time taken to reach equilibration is different for different initial startup configurations. To test this hypothesis, a relatively small scale simulation (with 4 surfactant monomer having only 3 carbons in the hydrophobic tail and the head similar to SDS) was already carried out and the organic molecule was introduced after an aggregation has been formed, after 5 ns of equilibration. The location of the organic molecule was changed in the system (outside the micelle) and three different initial configurations were tried. Only for the case of surfactant with benzene monomer has been analyzed and it is found that the molecule enters inside through the micelle surface taking around 15-25 ns of equilibration time depending on the initial configuration. The results obtained (potential and other energy terms) were similar to the case compared to the initial configuration with random placement of the organic molecule along with the surfactant monomers and water molecules.

However, the above analysis (with different initial configurations) could not be carried out for actual system (having 60 SDS monomer units) because of the large size of the system requiring extensive computational time and resource which is beyond the scope of the present study.

2.1 Calculation of free energy change

The free energy change is computed using the thermodynamic integration method employing a coupling parameter for switching transition from initial to final state in the thermodynamic process.[36] The hybrid Hamiltonian of the system is represented as,

$$H(\lambda) = H_0 + (1-\lambda) H_I + \lambda . H_F \qquad (2)$$

where, H_0 is the total Hamiltonian of the non-changing species of the system, H_I and H_F are Hamiltonian for initial and final state of the observed species. Here, λ is the coupling parameter corresponding to initial and final states for values and it varies between 0 and 1, respectively. In the thermodynamic integration, the Helmholtz free energy (ΔF) of the system is estimated by the following expression,[37]

$$\Delta F = F_{\lambda=1} - F_{\lambda=0} = \int_0^1 \left\langle \frac{\partial H(\lambda)}{\partial \lambda} \right\rangle_\lambda d\lambda \qquad (3)$$

The definite integration in Eq. (3) is done using quadrature method. In this implementation, the ensemble average is described by a cubic spline polynomial of λ and integrated analytically. Thermodynamic integration can be carried out by windowing, i.e., by performing discrete simulations with specified values of λ.[38] The ensemble averages are then calculated for each window and numerical integration is carried out using the trapezoidal rule. In the present study, integration is performed by slow-growth method, in which λ is varied gradually over the course of a single simulation.[39] The calculations are carried out using the TSM module in CHARMM using a linear coupling.[40] This slow growth method is

preferred since the steady continuous change in λ is a more stable way to achieve the transformation than the discrete jumps of the window method[41] and also in terms of minimal hysteresis on reversibility.[42] Slow growth is an approximation of the thermodynamic integration method that resembles ideal isothermal quasi-static process used in defining the free energy. In this method, instead of a constant λ for a given trajectory, the parameter is varied monotonically with each time step, as indicated,

$$\Delta F = \sum_{i=2}^{n-1} H\left(\lambda_i + \Delta\lambda_{i+1}\right) - H\left(\lambda_i\right) \quad (4)$$

where, λ_1 and λ_n are equal to 0 and 1, respectively. The integration is avoided at the end points (close to zero and one), since the partial derivatives are also zero for the initial and final states, which may lead to forces that approach a constant or zero value (zero potential energy) and thus atoms can have positions anywhere in the phase space.[43]

3.0 Results and Discussions

3.1 Simulation settings and choice of aromatic molecules

The total number of SDS molecules selected is 60, placed in 84 $\overset{o}{\text{A}}$ (edge length) cubic box. The box size and the number of water molecules are limited by the computational requirements. Thus, the resultant surfactant concentration is around 20 CMC. It has to be mentioned that the aggregation number of SDS for micelle formation varies from 55 to 75. At the beginning of the simulation, the organic molecule is placed in the center of the box and the surfactant molecules are uniformly distributed in the form of face-centered-cubic lattice spatial configuration. All water molecules in the vicinity (within 1 $\overset{o}{\text{A}}$) or overlapped with the organic molecule or the surfactant molecules are removed to avoid atomic clashes and

abnormal repulsive forces. Care is taken so that exactly same number of water molecules is deleted for the simulation of four different systems. The other relevant simulation settings are already described in section 2.0.

It has been reported in literature that the class of aromatic molecules having a benzene ring are considered most toxic compounds present in polluted water. Among them benzene, toluene, phenol and pyridine are common and present in significant proportion from various industrial discharges. Benzene features in the USEPA list of top 10 most hazardous contaminants present in drinking water.[44] Hence, the organic compounds studied in the simulation are selected based on their levels of toxicity and their presence in water.

The organic molecules are known to be solubilized in the inner hydrophobic core of the micelles (Fig. 1). However, the exact solubilization site depends on the extent of interaction and stability of such systems in the surfactant environment. Preliminary experimental results based on fluorescence time relaxation data, suggests that the locus of solubilization of organic molecules is in the inner core of the micelles.[45, 46] However, pinpointing the location experimentally to a fraction of a nanometer precision is not yet available. There are reports that state that polarizable hydrocarbons (short chain arenes) are solubilized by absorption at the micelle-water interface.[47] Several factors affecting the solubilization are: (1) polarizability of the π-electron cloud of the aromatic nucleus; (2) dipole-dipole interaction between the polar groups of the solubilizate and surfactant; (3) length and shape of hydrocarbon chain of the surfactant; (4) curvature of the micelle surface affecting the delocalization of the laplace pressure; (5) volume and asymmetry of the micelle. The molecular dynamics study not only aims to identify the location but can extract important thermodynamic information useful in interpreting the stability and interactions of the micelle-organic complex.

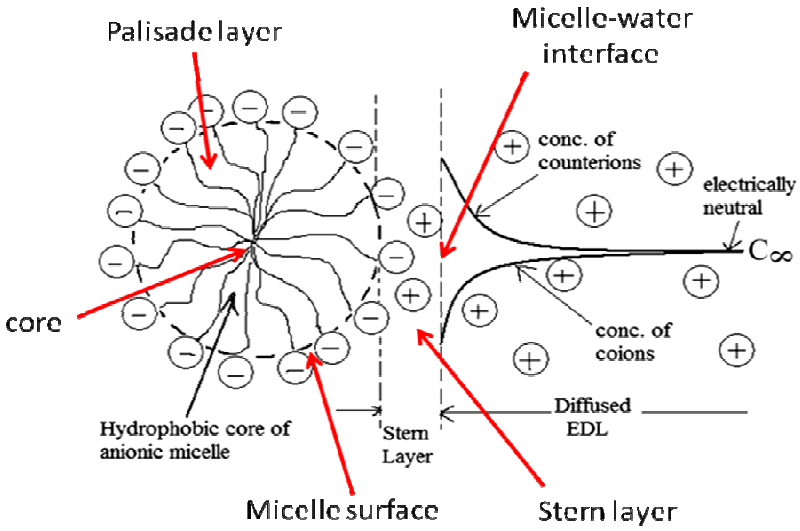

Fig 1: Schematic of the micellization process and potential sites of solubilization.

3.2 Potential energy of SDS-organic complex system

The evolution of the potential energy of the system is presented in the supplemental figure (Fig. S1). It has been found that after 2 ns of dynamic simulation, the system achieves equilibrium. One can observe that SDS-phenol is the most stable system among the four aromatic molecules. The potential energy of the phenol and toluene are similar because of similar size, however, the overall energy of phenol-SDS complex is driven by electrostatic interactions and its solubility in water, while hydrophobic interactions are more prominent for solubilization of toluene. The peripheral environment of the SDS micelle is polar and charged, and it will be seen later that the location of phenol attachment is in the micelle-water interface (or can be even in the aqueous phase) while benzene is in the interior hydrophobic core of the micelle. So, the location of solubilization site determines the overall potential energy of the system.

3.3 Interaction energies of the SDS-organic complex system

The electrostatic interaction energies of the organic molecule-micelle systems are presented in Fig. 2(a). Pyridine and phenol exhibit more polar nature, compared to benzene and toluene. The relative polarity indices of the aromatic molecules are presented in Table 1. Phenol is most polar among these molecules, thus the electrostatic energy for phenol-SDS complex is the least. It must be noted that the anionic surfactant heads have negative polarity and are projected outwards facing the water molecules, thereby creating a negatively charged environment in the Stern layer. The resonance structures of phenol and pyridine reveal that the ring is negatively charged in case of the former while it is partially positive for the later. So, in case of pyridine, the ring is orientated towards the micelle surface with the nitrogen atom projected away. In case of phenol, the trend is reverse, with the oxygen atom is orientated towards the micelle surface. Hence, the electrostatic energy of phenol+SDS complex is less compared to pyridine+SDS. The electrostatic energies of toluene and benzene are similar, as both of them have similar polarity indices.

The van der Waals energies due to hydrophobic interactions are calculated based on the L-J potential (Eq. 1). The van der Waals interactions are order of magnitude less than the electrostatic interactions (Fig. 2b) because of the ionic nature of the micelle and some of the solutes. It can be observed that benzene has the least van der waals interaction energy and is, therefore, more stable in the hydrophobic environment. It can be observed from the evolution of the van der waals energy that there is hardly any change in interaction for phenol+SDS complex. This is due to the fact that phenol is polar (highest in the set of chosen molecules), and interaction is mostly dominated by electrostatics. Van der waals interaction is experienced by the hydrophobic tail of the surfactant in the micelle. Hence, in case of benzene, the hydrophobic interactions are prominent and it is more stable inside of the micelle.

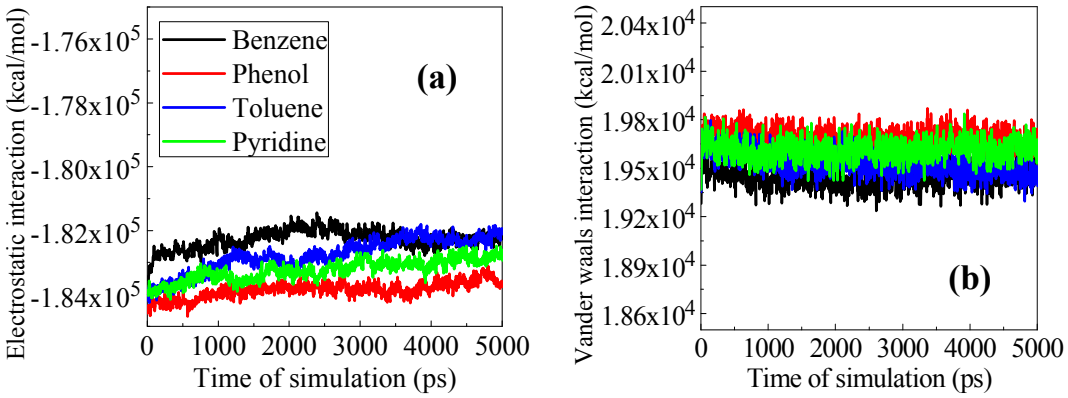

Fig. 2: Variation of the (a) overall electrostatic energy and (b) vander waals interaction energy with time of simulation.

3.4 Radial distribution function g(r)

The radial distribution function (Fig. 3a) provides important information about the density distribution of the surfactant in the vicinity of the center of mass of the aromatic molecules. It can be observed from this figure that the probability of finding surfactant head near phenol and pyridine sites of attachment (oxygen atom in case of phenol and the ring, particularly the para position in case of pyridine) is more at smaller distances. There is small peak in the region of 1.5 to 2 $\overset{o}{A}$ for phenol. This can be interpreted, that the oxygen atom of phenol is more approachable compared to bulkier ring of pyridine. The high fluctuations in the density distribution profile of pyridine molecule suggest that the partial negative charge over the nitrogen atom destabilizes the surfactant orientation in the micelle as the dipole moment of pyridine (2.2 D) is more than that of phenol (1.7 D), at large distances. Benzene and phenol exhibit similar g(r) profiles at larger distances, although the electrostatic energies are quite different for these systems. It can be concluded that phenol is located in the micelle-water interface (outwards the micelle) and benzene in the palisade layer (inwards), both sharing almost same distance from the surfactant head. This is also represented in Fig. 3(b), that clearly shows phenol and pyridine experience more water molecules around it than

benzene (or toluene). There is a small peak at a small distance (less than $2\,\overset{o}{\mathrm{A}}$) for phenol, indicating there exists a hydration of the phenol ring, even though pyridine is most hydrophilic among these four solutes. This observation is also in accordance with the fact, that the dynamics of water molecules is different in Stern layer than that in the bulk.[48] Toluene in both the figures has minimum probability of surfactant head or water molecule, implying it is buried further deep in the hydrophobic core.

Among the four molecules, the dielectric constant of pyridine is the highest (ε_r for pyridine, phenol and toluene are 13.2, 8.0, 2.5 and 1.8, respectively). With increase in dielectricity, the electrical potential distribution of the charged negative interface (micelle surface) is diffused, as the EDL thickness is proportional to $\varepsilon_r^{1/2}$. Assuming that the organic molecules are point charges and neglecting plane (micelle surface) – sphere (organic molecule) EDL interaction, the charge distribution will be affected by the relative potential distribution in the EDL. The electrical charge density of pyridine will be more because of its high dielectric properties, which is observed in this case (Fig. 3a). Another interesting observation from Fig. 3(b) is that local density distribution$\left[\rho(r)=\rho_{bulk}g(r)\right]$ of phenol and pyridine is similar, in relation to their bulk densities (Density of pyridine is 982 and phenol is 1070 kg/m^3), because of same molar concentration. However, the local density distribution is affected in the neighborhood of the charged interface as evident from Fig. 3a. The diffusivity of Pyridine ($0.76\text{x}10^{-9}$ m^2/s) is less compared to phenol ($1.013\text{x}10^{-9}$ m^2/s). This suggests that smaller mean displacement of the pyridine molecules from its equilibrium position, supporting the fact, that the presence of pyridine is enriched around the micelle surface than phenol.

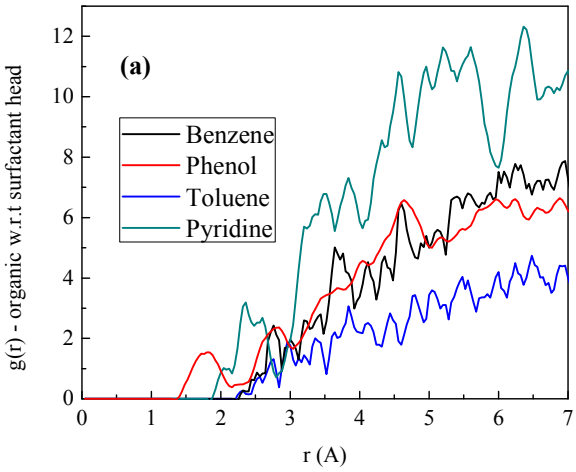

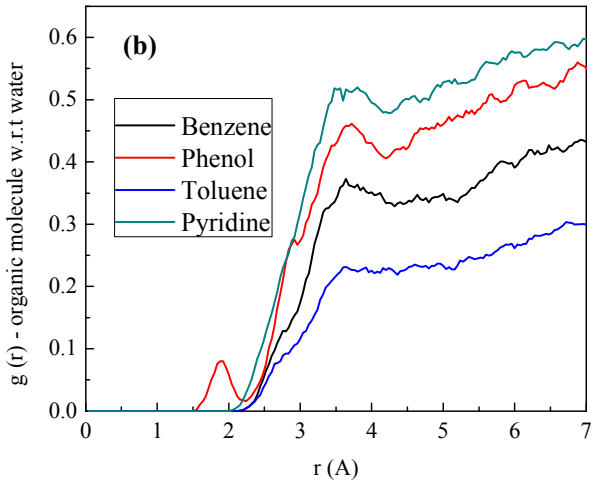

Fig. 3: Radial Distribution function g(r) of center of mass of the aromatic molecule with respect to (a) surfactant head and (b) water molecule.

3.5 Interpretation of the separation distance

Fig. 4 describes that both toluene and benzene do not reside in the center (or center of mass) of the micelle. In that case, we can expect a unimodal distribution of the surfactant head locations equivalent to the radius of the micelle. The fractional distribution of surfactant heads in the region of 25 to 35 $\overset{o}{A}$ is high compared to other distances for benzene and

toluene. The size of the anionic micelle varies from 40 to 50 $\overset{o}{A}$, depending on the presence of another solute.[49] So, the benzene and toluene molecules appear to be solubilized inside the core and approximately 10 $\overset{o}{A}$ deep from the outside surface. Since, the size of toluene molecule is larger than benzene, the overall micelle size is larger in case of SDS-toluene system than SDS-benzene micelle. The spatial distribution pattern of surfactant head for phenol is peculiar, as the distribution pattern is uniform at all length scales. This suggests that the shape of the micelle is distorted to a certain extent and it has probably deformed into a stretched ellipsoid and phenol being located in the outer region, the Stern layer. This is also corroborated with the observations from Fig. 3(a), that at smaller distance, there is a small peak for phenol+SDS system. The distribution profile for pyridine shows that there is peak localization of the heads in the range of 50 to 60 $\overset{o}{A}$. This is possible, if pyridine is present in the micelle-water interface. The pyridine ring exhibits attractive force to the surfactant heads distorting the micelle shape and presumably converts into a curved conical shell, with the tip pointed towards the aromatic molecule. This fact is also supported by the increased hydration number of pyridine molecule (Fig. 5). However, the distorted shape can also be modified depending on the relative molar concentration of the surfactant and organic solute. If the ratio of the molar concentration of organic solute to surfactant is higher than the micellar aggregation number at a particular temperature, the shape and the subsequent solubilization can be severely affected in case of pyridine and phenol. Such observations were also reported by Kandori et al.[15] experimentally.

To quantify the micelle size, further investigation is probed. The surfactant head group position has been identified and the distances between any two monomer heads are computed (total ${}^{n}C_2$ number of distances are calculated, where n is the micellar aggregation number) of the equilibrated micelle complex structure. The distances which are larger than or

equal to twice the monomer chain length are selected and the average is taken as the micelle diameter. In case of SDS-phenol system, distance from the phenol center to the surfactant heads are selected and the average of the distance larger than the twice of the monomer length is calculated. The micelle diameter calculated for different systems are obtained as:

Organic (SDS micelle)	*Micelle size (A)*
benzene	41.3±2.1
toluene	48.1±1.8
phenol	50.4±2.7
without the organic	35.7±1.1

It may be noted that the micelle size without any organic solubilization obtained in the present calculation is close to the experimental observed value of 34-40 A, reported in various studies.

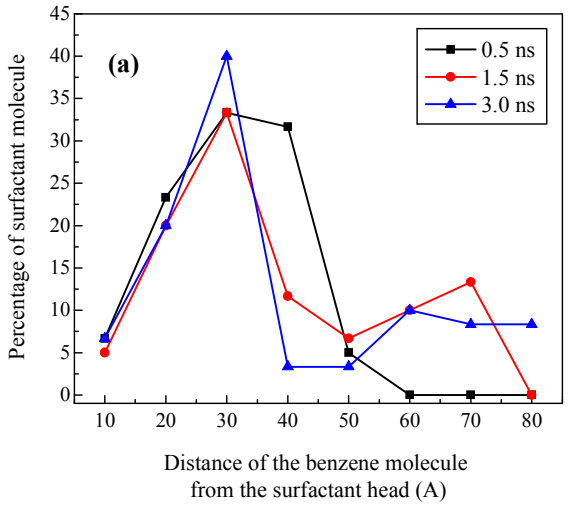

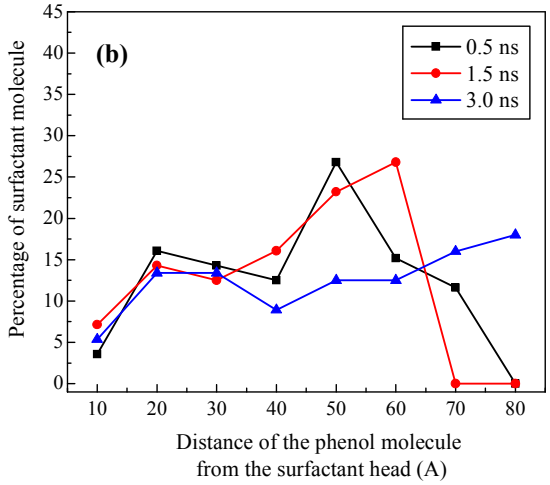

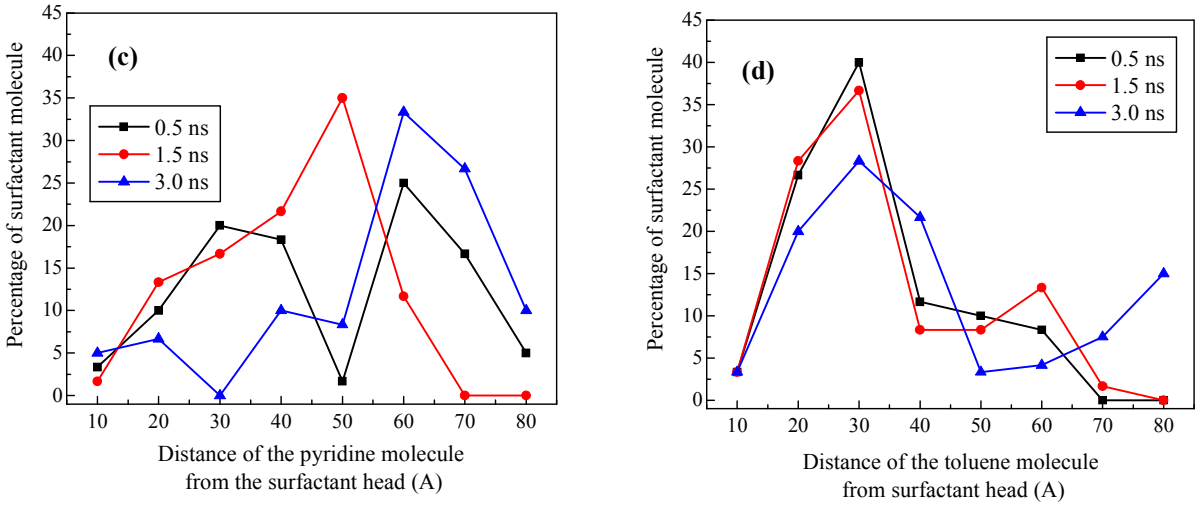

Fig. 4: Spatial distribution of the fraction of surfactant molecules (head) from the (a) benzene, (b) phenol, (c) pyridine and (d) toluene molecule.

3.6 Hydration number and solvent accessible free surface area

The hydration number represents the statistically significant number of water molecules in the neighborhood of the organic molecule at different distances from its center. As expected, pyridine shows maximum hydration number at any location compared to the other molecules. This further consolidates that pyridine is located towards the outer region and expresses more hydrophilic behavior compared to benzene and toluene, as shown in Fig. 5. The average number of water molecules around phenol (at $10\,\overset{o}{\text{A}}$) is 150 followed by benzene having 120 and least is by toluene. The hydration number fluctuates heavily during the course of the simulation suggesting that the aromatic molecule undergoes rigorous self-orientation to attain a minimum energy configuration, which is probably owing to its large size. The figure also suggests that hydration number is almost zero at $2.5\,\overset{o}{\text{A}}$ even though the minimum cut-off distance for the repulsion region in the L-J potential is set at $1\,\overset{o}{\text{A}}$. This implies that the π-electron density, due to benzene ring in the aromatic molecule does not

allow any water molecule to interact within 2.5 $\overset{o}{A}$. This figure reaffirms that pyridine is present in the micelle-water interface and toluene is located a bit deeper inside the hydrophobic core. This result is also in correspondence to the log P values (the log P values are the measure of hydrophobicity of the molecule and are calculated based on the partition co-efficient of the octanol-water system) and the solubility constants (Henry's constant of solubility) of different molecules, presented in Table 1. Pyridine has the lowest log P value indicating that it is the least hydrophobic while toluene has the highest log P value. The rate of dissociation (in terms of pKa values) is much higher for pyridine (5.25) compared to phenol (9.95). At neutral pH, pyridine is more dissociated compared to phenol. Also, the solubility of pyridine molecule is higher than phenol at a particular temperature (as referred from the logP values in Table 1). The affinity of the pyridine molecule towards water is highest among the four selected molecules. The dipolar intermolecular force between the pyridine and water molecule is more compared to phenol. The magnitude of δ_p^2 (polar component of Hansen solubility parameter) is 8.8 for pyridine while 5.9 for phenol. To the authors' knowledge, the above mentioned facts are responsible describing the possible interaction and favorable location of solubilization of the phenol and pyridine outside the micelle.

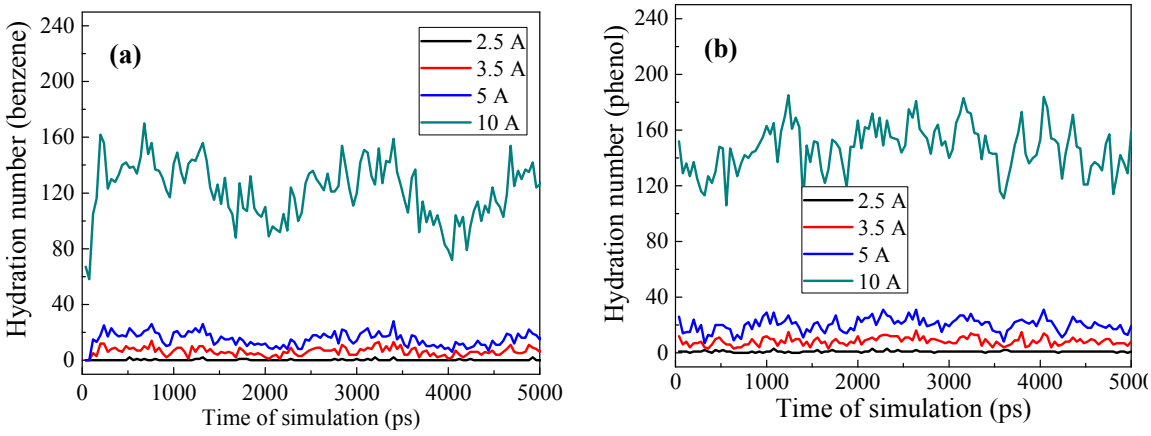

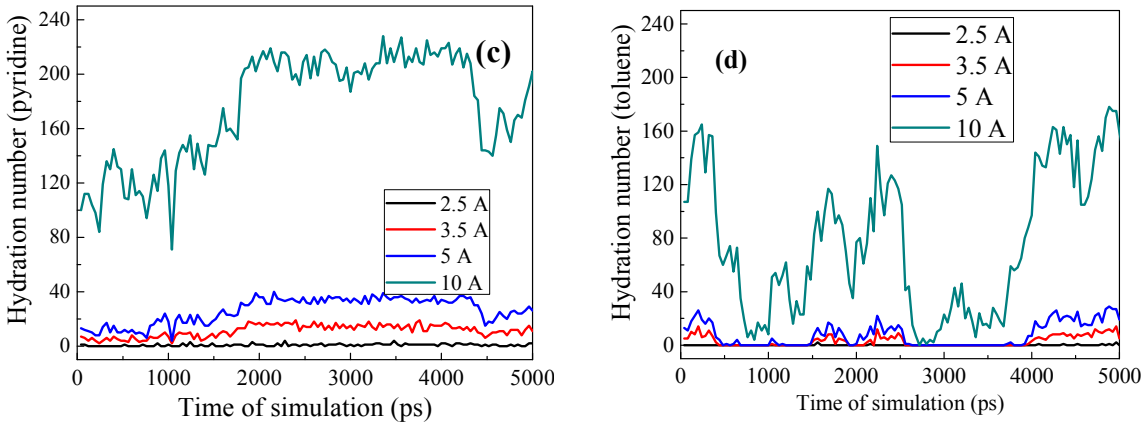

Fig. 5: Hydration number of the organic molecule at various distances from its center (a) benzene, (b) phenol, (c) pyridine and (d) toluene.

The solvent accessible free surface area describes the area accessible to the solvent molecules (water in this case) and has been calculated using the SASA implicit solvent model[50] in CHARMM.[24] The solvent accessible free surface area of different molecules is presented in Fig. 6. The maximum available area for pyridine suggests that it is slightly away from the outer layer, micelle-water interface and a pointed conical tip of surfactant head is projected towards it, thereby a large portion of it is accessible to water molecules. However, one may wonder how the toluene molecule has more accessible area than phenol. Phenol is located in the Stern layer and the ring is orientated away from the surfactant head. The presence of phenol distorts the shape of the micelle (as already explained in the discussion of Fig. 4), thereby reducing the accessible surface area. The toluene molecule as suggested is solubilized a bit deep in the hydrophobic core. One must remember here, that in central region of ionic micelle, there is a vacant space as the tails do not extend to the center in order to the accommodate more surfactant monomer units in the micelle. Even though the central region is inaccessible to the water molecules, the toluene (probably exists there) has more surface area uncovered by the surfactant molecules. This is reflected in the calculation of the

solvent accessible area. Benzene is solubilized in the palisade and hardly has any accessible area, as it is completely screened by the tails of the surfactant monomers.

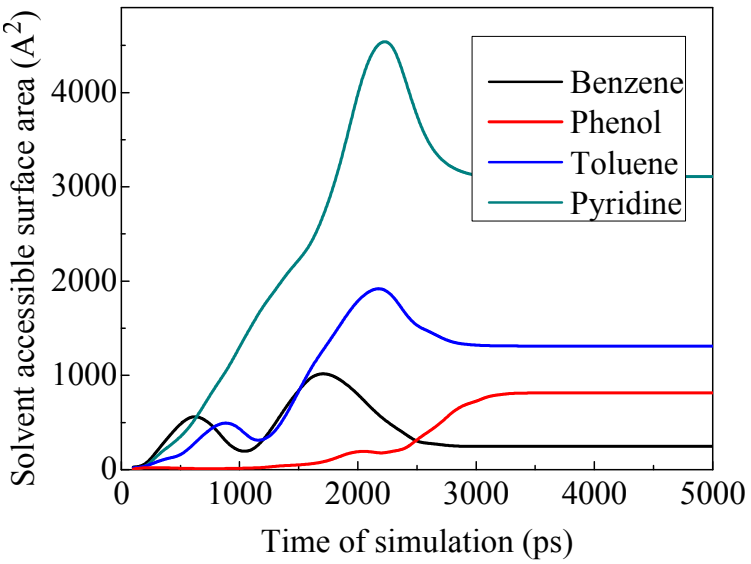

Fig. 6: Solvent accessible free surface area for various organic molecules.

3.7 Free energy change

The initial state for the free energy calculation is defined as the aromatic molecule dispersed in the bulk water with 30A away from the micelle surface. The final state is the location of the aromatic molecule in the vicinity (neighborhood or inside the micelle depending on the type of molecule) of the micelle where it is placed after the 5 ns equilibration. For the initial state, the aromatic molecule inside the micelle is replaced by dummy atoms whereas in the final state, the aromatic molecule in the water (bulk) phase is replaced by water molecules. The reversible path of the slow growth thermodynamic integration process, from the initial to final state is also calculated by swapping the initial and final configuration, and the average value (forward and reversible path) for the free energy change is reported. Total 20 intervals within the range of 0 (initial) to 1 (final), each of 100ps duration is computed, so as to allow complete equilibration of the perturbed intermediate steps. The temperature is maintained at 300 K during the free energy calculation.

The free energy and entropy change show that toluene and phenol are the least solubilized as observed from Table 2. The reasons being charge interaction of the phenol with the surfactant head (opposite polarity) and its location in the micelle-water interface.[51] The micellar enhanced ultrafiltration of phenol in anionic and cationic micelles shows that solubilization of phenol is significantly higher in cationic micelles.[52] In case of toluene, because of its higher molecular volume, solubilization is restricted,[13] even though it is solubilized deep inside the hydrophobic core. The entropy and free energy change for benzene suggests that it is solubilized maximum and in the palisade layer (as discussed earlier). Pyridine being present in the micelle-water interfaces, having high hydration number; it is more stable in the hydrophilic environment. This is reflected in the free energy change values for pyridine, which is in sharp contrast to the binding efficiency with the micelle.

Table 2: Results of the free energy simulation.

Molecule	Helmholtz free energy change: ΔA (kcal/mol)	Entropy change : ΔS (kcal/ mol. K)
Benzene	-492.9	3041.9
Toluene	-223.0	1225.0
Phenol	-245.5	1257.4
Pyridine	-446.4	2530.3

Conclusion

The present study attempts to calculate and interpret various thermodynamic and geometrical information of different surfactant-organic complex. The molecular self-assembly is severely affected by the presence of organic molecules in the system. Following are the concluding remarks based on the results of the simulation:

(1) The solubilization of toluene is deep in the hydrophobic core of the micelle, benzene is solubilized in the palisade layer, phenol is in the Stern layer and pyridine in the micelle-water interface outside the micelle.

(2) The mechanism of toluene and benzene solubilization is purely by hydrophobic interactions, while that of pyridine and phenol are electrostatic due to polar nature of these organic molecules.

(3) The aromatic ring in phenol is negatively charged while the surfactant heads are negatively charged (SDS is an anionic surfactant), leading to the orientation of the phenol ring away from the micelle due to dipole-dipole interaction.

(4) The nitrogen atom in pyridine has partial negative charge and therefore, it is strongly repelled from the micelle surface and is located in the micelle-water interface, having high hydration number.

(5) The charged aromatic molecule distorts the shape of the micelle and also influences the distribution of water molecule around the micelle. This appears reasonable as the behavior of water molecule around a micelle is different as mentioned in literature.[9]

(6) The size of SDS-phenol and SDS-toluene complex is higher than SDS-benzene system. Experimental observations reported also reveal similar behavior.[52]

(7) The size of non-polar aromatic molecule hinders the diffusion of it into the hydrophobic core.

(9) The free energy change of SDS-pyridine system is maximum and the least for toluene.

References

[1] S. Jalili and M. Akhavan, *Colloid Surf. A: Physiochem. Eng. Asp.*, 2009, **352**, 99-102.

[2] F. Palazzesi, M. Calvaresi and F. Zerbetto, *Soft Matter*, 2011, **7**, 9148-9156.

[3] A.H. Poghosyan, L.H. Arsenyan, H.H. Gharabekyan, S. Falkenhagen, J. Koetz and A.A. Shahinyan, *J. Colloid Interface Sci.* 2011, **358**, 175-181.

[4] H. Dominguez, *J. Phys. Chem. B* 2007, **111**, 4054–4059.

[5] H. Dominguez and M.L. Berkowitz, *J. Phys. Chem. B*, 2000, **104**, 5302–5308.

[6] N.R. Tummala and A. Striolo, *ACS Nano*, 2009, **3**, 595–602.

[7] M. Luo and L.L. Dai, *J. Phys.: Condens. Matter*, 2007, **19**, 375109.

[8] M. Sammalkorpi, A.Z. Panagiotopoulos and M. Haataja, *Phys. Chem. B*, 2008, **112**, 2915–2921.

[9] C.D. Bruce, S. Senapati, M.L. Berkowitz, L. Perera and M.D.E. Forbes, *J. Phys. Chem. B*, 2002, **106**, 10902-10907.

[10] C.D. Bruce, S. Senapati, M.L. Berkowitz, L. Perera, and M.D.E Forbes, *J. Phys. Chem. B*, 2002, **106**, 3788-3793.

[11] S. Karaborni, N.M. van Os, E. Esselink and P.A.J. Hilbers, *Langmuir*, 1993, **9**, 1175-1178.

[12] N. Sarkar, A. Datta, S. Das and K. Bhattacharyya, *Phys. Chem.*, 1996, **100**, 15483-15486.

[13] F. Gadelle, W.J. Koros, and R.S. Schechter, *J. Colloid Interface Sci*., 1995, **170**, 57-64.

[14] P. Lianos, M.L. Viriot and R. Zana, *J. Phys. Chem*. 1984, **88**, 1098-1101.

[15] K. Kandori, R.J. McGreevy and R.S. Schechter, *J. Phys. Chem*. 1989, **93**, 1506-1510.

[16] S. Mondal, S. Ghosh and S. De, *Langmuir*, 2012, **28**, 11329−11336.

[17] S. De and S. Mondal, *Micellar Enhanced Ultrafiltration: Fundamentals and Applications*, Taylor & Francis, Boca Raton, 2012.

[18] G.A. Smith, S.D. Christian, E.E. Tucker and J.F. Scamehorn, *ACS Symposium Series*, 1987, pp. 184-198.

[19] L.J. William, C. Jayaraman, D.M. Jeffry, W.I. Roger and L.K. Michael, *J. Chem. Phys.*, 1983, **79**, 926–935.

[20] W.L. Jorgensen, J. Chandrasekhar, J.D. Madura, R.W. Impey and M.L. Klein, *J. Chem. Phys.*, 1983, **79**, 926–935.

[21] J.B. Klauda, R.M. Venable, J.A. Freites, J.W. O'Connor, D.J. Tobias, C.M. Ramirez, et al., *J. Phys. Chem. B*, 2010, **114**, 7830–7843.

[22] K. Vanommeslaeghe and A.D. MacKerell Jr, *J. Chem. Inf. Model.*, 2012, **52**, 3144-3154.

[23] K. Vanommeslaeghe, E.P. Raman and A.D. MacKerell Jr, *J. Chem. Inf. Model.*, 2012, **52**, 3155-3168.

[24] B.R. Brooks, C.L. Brooks III, A.D. Mackerell, et al., *J. Comp. Chem.*, 2009, **30**, 1545-1614.

[25] C. Reichardt, *Chem. Soc. Rev.*, 1994, **94**, 2319-2358.

[26] J. Sangster, *J. Phys. Chem. Ref. Data*, 1989, **18**, 1111-1227.

[27] C.S. ChemBioDraw Ultra, *Cambridge Soft corporations*, v11.0.

[28] U. Essmann, L. Perera, M.L. Berkowitz, T. Darden, H. Lee and L.G. Pedersen, *J. Chem. Phys.*, 1995, **103**, 8577-8593.

[29] J.P. Ryckaert, G. Ciccotti and H.J.C. Berendsen, *J. Comp. Phys.*, 1977, **23**, 327–341.

[30] C. Gonzalez and H.B. Schlegel, *J. Chem. Phys.*, 1989, **90**, 2154-2161.

[31] J.W. Chu, B.L. Trout and B.R. Brooks, *J. Chem. Phys.*, 2003, **119**, 12708-12717.

[32] D.C. Rapaport, *The Art of Molecular Dynamics Simulation*, Cambridge University Press, Cambridge, 2004.

[33] M.T. Hyvoven and P.T. Kovanen, *J. Phys. Chem. B*, 2003, **107**, 9102-9108.

[34] H.C. Andersen, *J. Chem. Phys*., 1972, **72**, 2384-2393.

[35] H.J.C. Berendsen, J.P.M. Postma, W.F. van Gunsteren, A. Dinola and J.R. Haak, *J. Chem. Phys*., 1984, **81**, 3684-3690.

[36] T.P. Straatsma, In *Reviews in Computational Chemistry*, ed. K.B. Lipkowitz, D.B. Boyd, John Wiley & Sons, New Jersey, vol. 9, 2007, p. 81.

[37] T.P. Straatsma and H.J.C. Berendsen, *J. Chem. Phys*., 1988, **89**, 5876-5886.

[38] M. Muller, K.C. Daoulas, *J. Chem. Phys*., 2008, **128**, 024903.

[39] H.J.C. Berendsen, J.P.M. Postma and W.F. van Gunsteren, In *Molecular Dynamics and Protein Structure*, ed., J. Hermans, Polycrystal Book service, Western Springs, IL, 1985, p. 43.

[40] D.J. Tobias and C.L. Brooks, *Chem. Phys. Lett*., 1987, **142**, 472-476.

[41] S. Boresch and M. Karplus, *J. Phys. Chem. A*, 1999, **103**, 119-136.

[42] H. Hu, R.H. Yun and J. Hermans, *Mol. Sim*., 2002, **28**, 67-80.

[43] T.P. Straatsma , Ph. D. thesis, University of Groningen, 1987.

[44] USEPA, National Primary Drinking Water Regulations, 2010, http://water.epa.gov/drink/contaminants/index.cfm#Primary

[45] R. Nagarajan and M.A. Chaiko, *J. Phys. Chem*., 1984, **88**, 2916-2922.

[46] M.J. Rosen, *Surfactants and Interfacial Phenomena*, John Wiley and Sons, Hoboken, 2004.

[47] M.J. Rosen, *Surfactants and Interfacial Phenomena*, John Wiley and Sons, Hoboken, 2004, pp. 180-182.

[48] S. Balasubramanian, S. Pal and B. Bagchi, *Curr. Sci*., 2002, **82**, 845-954.

[49] M. Almgren and S. Swarup, *J. Phys. Chem*., 1982, **86**, 4212-4216.

[50] S.J. Wodak and J. Janin, *Proc. Natl. Acad. Sci. USA*, 1980, **77**, 1736-1740.

[51] H. Adamczak, K. Materna, R. Urban´ski and J. Szymanowski, *J. Colloid Interface Sci*., 1999, **218**, 359–368.

[52] R.O. Dunn, J.F. Scamehorn and S.D. Christian, *Colloids Surf*., 1989, **25**, 49-56.

List of Figures

List of Tables

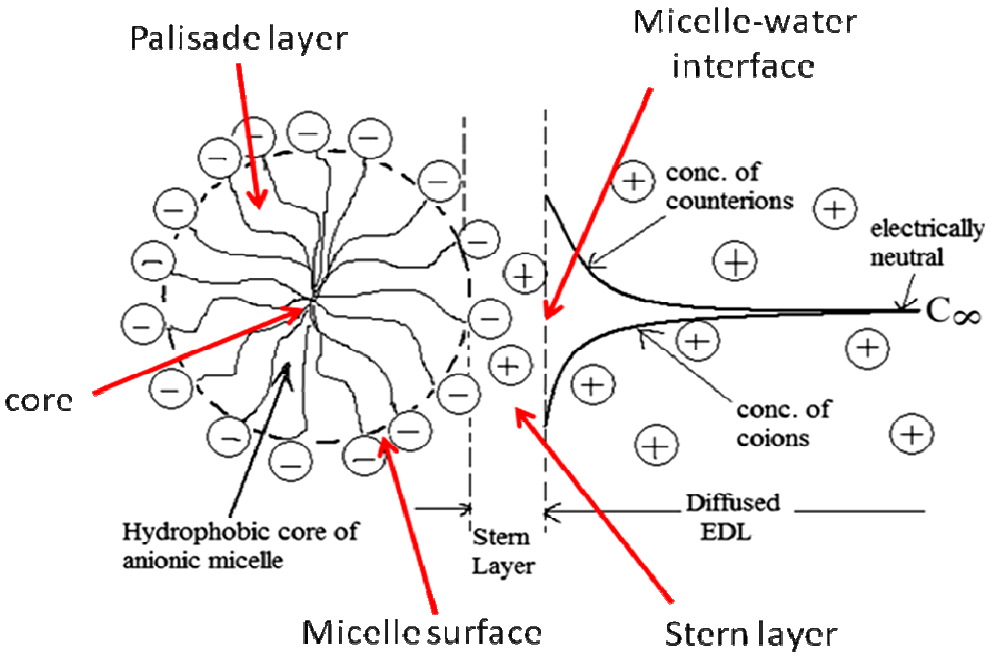

Benzene is solubilized in the palisade layer, toluene in the core (or towards the central region), phenol at the surface and pyridine in the micelle-water interface. Benzene and toluene are solubilized due to hydrophobic interactions, while for phenol and pyridine, it is mostly electrostatic interactions. During micellar enhanced ultrafiltration with anionic surfactant, phenol will have least rejection while benzene will have maximum, based on the results of the free energy change.